ELSEVIER

Polymer 42 (2001) 1533–1539

polymer

www.elsevier.nl/locate/polymer

# Electrical charge transport in polypyrrole/sulfated poly(β-hydroxyethers) blends

K. Kodama[a,*], T. Koshiba[b], H. Yamato[b], W. Wernet[c]

[a]*Chitose Institute of Science and Technology, 758-65 Bibi, Chitose, Hokkaido 066-8655, Japan*
[b]*Ciba Specialty Chemicals K. K., 10-66 Miyuki-cho, Takarazuka 665-8666, Japan*
[c]*Ciba Specialty Chemicals, Performance Polymers, R-1059. 7. 13, CH-4002 Basel, Switzerland*

Received 14 March 2000; received in revised form 12 May 2000; accepted 22 May 2000

**Abstract**

Electrical properties of polypyrrole/sulfated poly(β-hydroxyethers) (PPy/sulfated PHE), wherein the sulfated hydroxy groups in the latter component worked as dopants, were investigated, varying the doping level as well as the PHE molecular mass ($M_n$). The blends can be categorized into three groups: the slight-, moderate- and high-sulfation. In the moderate-sulfation, the charge transport above 80 K is characterized by the two-dimensional variable-range hopping (2D-VRH) through the PPy conducting channels formed on the surfaces of coiled PHE. In the high-sulfation, the dimensionality of the VRH changes from two to three. In addition, the carriers in the metallic states also participate in the charge transport. In the slight-sulfation, the hopping to the nearest neighbors operates in addition to the 2D-VRH. For all the samples, the dominant conduction below 80 K is the hopping governed by a Coulomb gap due to the electrostatic interaction between carriers. The change in the doping level causes the transition from one sulfation group to another when $M_n$ is large, whereas most blends are categorized into the moderate sulfation group when $M_n$ is small. This behavior is interpreted, considering the $M_n$ dependence of the spatial distributions of the PPy in the PPy/PHE blends. 

*Keywords*: Polypyrroles; Conductivity; Temperature dependence

## 1. Introduction

Electrically conducting polymers are a class of materials that have been intensively studied for almost two decades, aiming at applications for electromagnetic shielding, batteries, sensors, displays and so on. However, their practical use is still limited in spite of the variety of their electrical, electrochemical, optical and mechanical properties. A picture of an idealized conducting polymer is a one-dimensional chain of identical monomer units, whose π electrons are delocalized over the length of the chain in energy bands. However, there are several differences between the ideal and the real polymer. One of them is that the latter includes various types of structural disorders, which have considerable influences on its charge-carrier transport. A most critical one is the randomness in inter-chain distance which exists inherently in the real polymers with a macroscopic dimension. The charge transport in most conducting polymers, therefore, has been discussed in terms of theoretical models that have been developed originally for structurally disordered inorganic materials. Most of the models [1–8] can be conveniently summarized by the following equation

$$\sigma(T) = \sigma_0 \exp[-(T_0/T)^{1/n}], \quad (1)$$

where $\sigma_0$ is a moderately temperature-dependent pre-exponential factor, $T_0$ a characteristic temperature, $n$ usually an integer in the range 1–4, being dependent on details of hopping conduction processes.

The fact that structural parameters play crucial roles in the transport of conducting polymers provides us with a possibility in polymer blends like polypyrrole (PPy) doped with sulfated poly(β-hydroxyethers) (sulfated PHE) [9–11] or poly(*p*-styrenesulphonate) [12,13]. It may be possible to modify the parameters of the conducting networks such as their dimensionality and the inter-chain distances by changing the content and morphology, for example, of the polymeric dopants. The charge transport study on the PPy doped with poly(*p*-styrenesulphonate) [12,13] revealed that its transport was a function of the morphology of the latter component and that the variable range hopping (VRH)

* Corresponding author. Tel./Fax: +81-123-27-6062.
*E-mail address:* k-kodama@photon.chitose.ac.jp (K. Kodama).

0032-3861/01/$ - see front matter 
PII: S0032-3861(00)00396-7

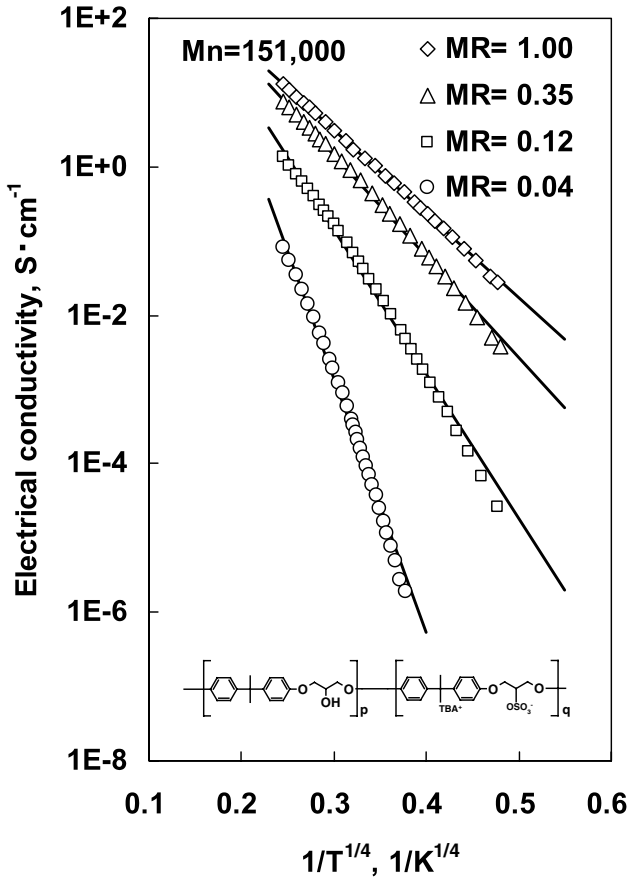


Fig. 1. Electrical conductivity for samples with $M_n = 151,000$ and MR = 0.04, 0.12, 0.35 and 1.00 as a function of $T^{-1/4}$. The inset to this figure is chemical structure of sulfated poly(β-hydroxyethers) (s-PHE). The sulfation ratio of the hydroxy groups in the PHE is expressed as $q/(p + q)$.

model was not applicable [12], unlike PPy doped with small counterions [14–22]. However, a systematic study on the transport of the PPy doped with polymeric dopants has not been reported yet.

In this paper, our results about the charge transport studies of the PPy/sulfated-PHE blends are reported. The PPy films are mechanically a little brittle, which can be improved drastically by being blended with PHE that has superior mechanical properties. The doping or sulfation ratio, $MR = p/(p + q)$, where $p$ and $q$ are the number of the sulfated and the unsulfated hydroxy groups in PHE chains, respectively, was systematically varied as well as the PHE molecular mass, $M_n$, in order to modify the spatial distribution of the PPy conducting channels. In this study, the temperature dependence of the DC conductivity was analyzed in terms of temperature dependence of the reduced activation energy, $W(T) = T\partial(\ln(\sigma^{-1}))/\partial(T^{-1})$, so that the parameter, $n$, which reflects the charge-carrier transport mechanisms is determined unambiguously. The results are interpreted in terms of the $M_n$ dependence of the spatial distributions of the PPy chains.

## 2. Experiment

The PPy/s-PHE blends were prepared as described elsewhere [9,10]. The PHE polymers were fractionated with acetone/tetrahydrofuran mixtures, which yielded the fractions having number-average molecular mass, $M_n = (\Sigma_i M_i \cdot n_i)/(\Sigma_i n_i)$, of 8500, 62,100 and 151,000, where $n_i$ is the number fraction of polymers in an interval of the mass histogram centered around the molecular mass $M_i$. Hydroxy groups in the PHE were then sulfated to varying degrees so that the sulfation ratios MR were in the range of 0.04–1. The PPy/s-PHE blends were synthesized galvanostatically at room temperature on a stainless steel electrode in a solution of sulfated PHE (s-PHE), pyrrole and water in propylene carbonate. The thickness of the prepared films was about 100 μm. After the synthesis, the films were rinsed in propylene carbonate and extracted with ethanol, and then dried in vacuum at 50°C for 12 h to remove water and propylene carbonate remaining in the films. It seems that the amount of water and propylene carbonate remaining in the films after the treatment is little, judging from the result of elemental analysis for the heat-treated films.

Chemical analysis of the sulfur to nitrogen ratio was carried out to reveal that the content of PPy in the blends varied from 3% for samples with MR = 0.04 to 35% for samples with MR = 1. The doping level was in the range of 0.35–0.21 electrons per PPy ring, depending mainly upon MR.

A section of $5 \times 20$ mm$^2$ was cut from each film, and Au electrodes of 100 nm thickness were deposited with a vacuum evaporator for conductivity measurements. The four-probe method was used for the measurement. The conductivity was measured in the temperature range 20–270 K, using a closed cycle refrigerator system. The electric power dissipated in the samples was kept low enough to avoid the effect of Joule heating.

## 3. Results and discussion

### 3.1. Evaluation of parameter n

Typical results of the conductivity are presented as a function of $T^{-1/4}$ in Fig. 1 for the PPy/s-PHE blends with $M_n = 151,000$ and MR = 0.04 − 1. The solid lines are the best fit for the experimental results determined with the least square method. The experimental results, for MR = 0.12 and 0.35 in particular, show a curvature in the log($\sigma$) vs. $T^{-1/4}$ plot, thus indicating that the dependence cannot be described with a single $n$ value in the whole temperature region. Therefore, temperature dependence of the reduced activation energy, $W(T) = T\cdot\partial(\ln \rho)/\partial(T^{-1})$ [23], was calculated from the experimental results for all the samples in order to determine the parameter $n$ and make unambiguous distinctions among transport mechanisms. The parameter $n$ in Eq. (1) was then determined with the least square

Table 1
Parameters describing charge transport properties. $\sigma_{RT}$ stands for the room-temperature conductivity, $n$, $\sigma_0$ and $T_0$ for the parameters in Eq. (1), $N_F$ for the density of the states at the Fermi energy expressed as Eq. (3), and $E_a$ for the activation energy in Eq. (5). The values marked with # on the right shoulder were determined to give the best fit to the experimental results below 80 K

| Category | $M_n$ | MR | $\sigma_{RT}$ $(\Omega\ cm)^{-1}$ | $n$ | $T_0$ (K) | $\sigma_0$ $(\Omega\ cm)^{-1}$ | $N_F$ ($\times 10^{20}$ 1/eV $cm^3$) | $E_a$ (meV) |
|---|---|---|---|---|---|---|---|---|
| *High sulfation* | 8500 | 1.00 | 18.6 | 5.14 | 197,000 | 3200 | 11.3 | – |
| | 62,100 | 1.00 | 14.4 | 5.45 | 365,000 | 5200 | 6.07 | – |
| | 151,000 | 1.00 | 15.6 | 8.82 | 621,000 | 13,000 | 3.57 | – |
| *Moderate sulfation* | 8500 | 0.35 | 8.47 | 2.91 | 25,600 | 770 | – | – |
| | 8500 | 0.12 | 5.78 | 3.02 | 25,100 | 450 | – | – |
| | 8500 | 0.04 | 4.64 | 2.87 | 26,100 | 440 | – | – |
| | 62,100 | 0.35 | 8.40 | 3.07 | 28,400 | 890 | – | – |
| *Slight sulfation* | 62,100 | 0.12 | 0.95 | 2.14 | 14,8000 | 1950 | – | 42.3 |
| | 151,000 | 0.12 | 1.69 | 2.30 | 90,000 | 1140 | – | 37.0 |
| | 151,000 | 0.04 | 0.12 | 1.72 | 525,000 | 10,600 | – | 71.5 |

method, using Eq. (2)

$$\log W(T) = \frac{1}{n}\log T_0 + \log\left(\frac{1}{n}\right) - \frac{1}{n}\log T. \quad (2)$$

The $n$ values thus obtained are given in Table 1. Most samples investigated have a break point around 80 K in the $\log[W(T)]$ vs. $\log(T)$ plot, as shown in Fig. 2(a), indicating that different values can be defined for $n$ below and above 80 K. For three samples with large $M_n$ and low MR, the plot gives straight lines and single $n$ values can be apparently defined in the whole temperature range, as in Fig. 2(b). However, their transport can be shown to be a combination of, at least, two conduction mechanisms.

The samples can be divided into three categories according to the $n$ values: highly, moderately and slightly sulfated samples. In the moderately sulfated samples, the $n$ values obtained above and below 80 K are close to three and two, respectively. The values for the highly sulfated samples are in the range 5.1–8.8 above 80 K and in the range 2.6–2.7 below 80 K. The slightly sulfated samples have apparently single $n$ values, ranging from 1.7–2.3, over the whole temperature range, though their transport is a combination of, at least, two different conduction mechanisms.

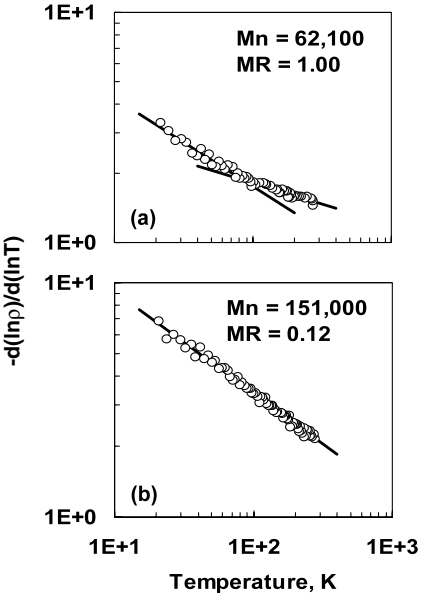


Fig. 2. The log (reduced activation energy) vs. log $T$ plots. For the sample with $M_n = 62,100$ and MR = 1.00, a breakpoint is clearly recognized around 80 K, whereas the plot gives a straight line over the whole temperature range for the sample $M_n = 151,000$ and MR = 0.12. The $n$ values obtained from this plot are given in Table 1.

### 3.2. Charge transport above 80 K in moderately sulfated PPy/s-PHE

The moderately sulfated samples have an $n$ value of 2.9–3.1 above 80 K. This value indicates that the charge transport is the 2D-VRH [3]. A typical result is shown as a function of $T^{-1/3}$ in Fig. 3(a). The straight line in the figure is the best fit of $\sigma(T) = \sigma_0 \exp[-(T_0/T)^{1/3}]$ to the experimental results above 80 K, that was determined with the least square method. The values of $\sigma_0$ and $T_0$ that give the best fit are summarized in Table 1.

The 2D-VRH transport in moderately sulfated samples can be understood, considering the morphology of PHE in solvents based on polymer solution theories [24]. From polymer solution theories, we can think of a polymer chain in a solvent as a coiled structure, where, in the better solvent, the more expanded and disentangled the coil becomes. Considering this, we can imagine the PHE as a coiled structure during sulfation (and PPy/s-PHE polymerization), wherein it is statistically anticipated that the hydroxy sites on the exterior will be preferentially sulfated, as compared to the hydroxy sites situated in the interior. Furthermore, this effect would be more pronounced for polymers with low MR. The attractive electrostatic interaction, that works between the oxidized PPy chains and the negatively charged sulfated segments of the PHE, makes the PPy chains situated close to the sulfated segments, thereby forming the 2D conductive channel on the s-PHE surface.

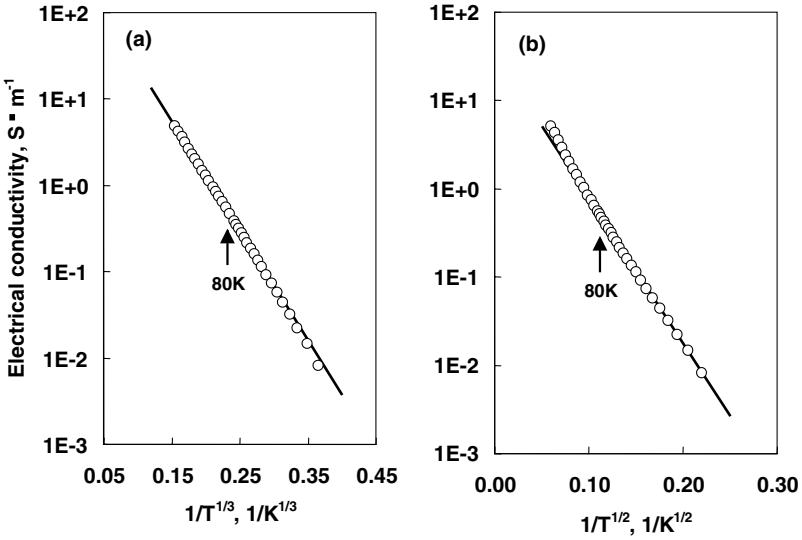


Fig. 3. The electrical conductivity of the sample with $M_n = 8500$ and MR = 0.12 as a function of (a) $T^{-1/3}$ and (b) $T^{-1/2}$. The straight lines are the best fits to the experimental results (a) above 80 K and (b) below 80 K, determined with the least square method.

### *3.3. Charge transport above 80 K in highly sulfated PPy/s-PHE*

The *n* parameter in Eq. (1) is usually smaller than four for structural-disorder-dependent transport. The *n* values are in the range 5.1–8.8 above 80 K for the highly sulfated samples, thus indicating the participation of a second charge transport mechanism, which is different from those governed by structural disorders. Therefore, it is supposed that the charge transport above 80 K in the highly sulfated samples is expressed as $\sigma_{measured} = \sigma_{VRH} + \sigma_{metal}$. The first term in the right side of the equation is clearly ascribed to the VRH. In the analysis given below, the VRH on the highly sulfated samples is assumed to be three-dimensional (3D), because most of the hydroxy groups are expected to be sulfated in these samples. The second component, $\sigma_{metal,}$ should be characterized by the reduced activation energy with weak temperature dependence, as compared to the 3D-VRH, to give the overall *n* value larger than four. The $\sigma_{metal}$ component, consequently, is treated as being temperature-independent in this analysis.

Then the $\sigma_{metal}$ value was optimized so that the temperature-dependent component, $\sigma_{VRH,}$ was expressed as $\ln(\sigma(T)) \propto -T^{-1/4}$. The $\sigma_{VRH}$ component obtained in this way is shown in Fig. 4 as a function of $T^{-1/4}$. The straight line is the best fit of $\sigma_0 \exp[-(T_0 - T)^{1/4}]$ to the $\sigma_{VRH}$ component above 80 K. The values of $\sigma_0$ and $T_0$ that give the best fit are given in Table 1.

In order to confirm the compatibility of $T_0$ and $\sigma_{VRH}$ thus obtained with the results previously reported for PPy, we calculated the room-temperature conductivity of the VRH component, $\sigma_{RT,VRH}$, with $\sigma_0$ and $T_0$ obtained above and investigated the correlation between $T_0$ and $\sigma_{RT,VRH}$. It has been known that the $T_0$ vs. $\sigma_{RT,VRH}$ plot for various types of structurally disordered materials gives a single curve [25]. The result is shown as the inset to Fig. 4. The compatibility can be clearly recognized between the results of this study and the data reported previously. This shows that the assumption is valid and that the temperature-independent conduction is in operation in parallel with the 3D-VRH in highly sulfated samples.

A plausible mechanism for the component $\sigma_{metal}$ is a metallic one. The participation of the carriers in the metallic states in parallel to the VRH is often concluded or proposed even when negative temperature dependence of the resistivity is observed. For example, temperature dependence of the resistivity of $H_2SO_4$-doped thiophene was similarly explained, assuming the conduction in the metallic states in parallel to 3D-VRH [27]. The room-temperature conductivity of this polythiophene is reported to be 11 S cm$^{-1}$, that is similar to or even smaller than those of the highly sulfated PPy/s-PHE blends. Therefore, it is reasonable to assume the metallic conduction in them.

### *3.4. Charge transport below 80 K in moderately and highly sulfated PPy/s-PHE*

The *n* value below 80 K for the moderately sulfated samples is in the range 2.2–2.4, which indicates that their conductivity can be expressed as $\sigma(T) = \sigma_0 \exp[-(T_0/T)^{1/2}]$. The conductivity of the sample with $M_n = 8500$ and MR = 0.12 is plotted against $T^{-1/2}$ in Fig. 3(b). The straight line in the figure is the best fit of $\sigma_0 \exp[-(T_0/T)^{1/2}]$ for the experimental results below 80 K. The values of $T_0$ and $\sigma_0$ giving the best fit are summarized in Table 1. The conductivity of the highly sulfated samples can also be interpreted similarly, though the *n* values obtained are a little larger than two.

The Coulomb gap model based on the electrostatic interaction between the charge carriers [4] can consistently

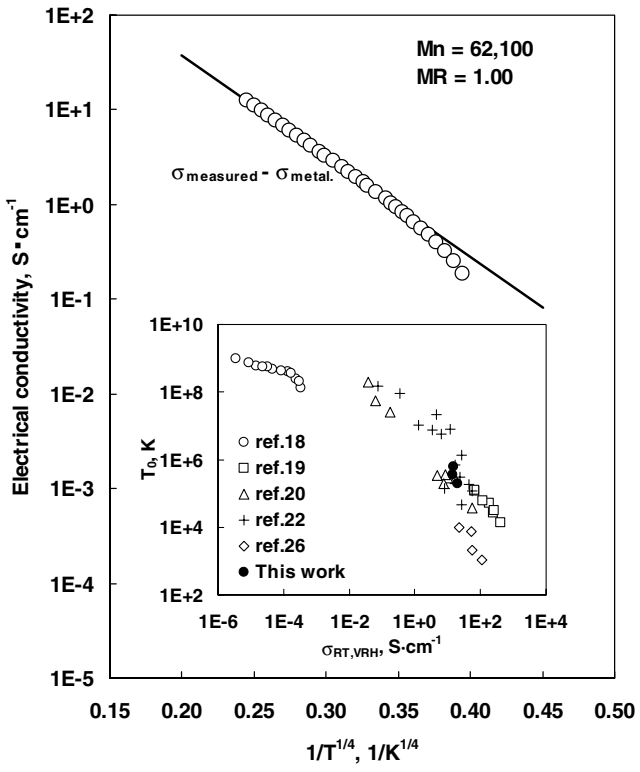


Fig. 4. The VRH component for the sample with $M_n = 62,100$ and MR = 1.00, which is obtained by subtracting the temperature-independent $\sigma_{metal}$ component from the $\sigma_{measured}$, as a function of $T^{-1/4}$. The inset to the figure is the $T_0$ vs. $\sigma_{RT,VRH}$ plot [18–20,22,26].

explain the experimental results. In this model, the Coulomb gap plays an important role in the low-temperature DC conductivity, and its influence can be neglected at higher temperatures, where the VRH is dominant. This transition between 3D-VRH and the hopping governed by the Coulomb gap occurs at $T_C$, which can be expressed as

$$T_C = \frac{e^4 N_F}{(4\pi\epsilon_0\epsilon_r)^2 \alpha k_B}, \quad (3)$$

where $e$ is the electronic charge, $\epsilon_0$ the permittivity of vacuum and $\epsilon_r$ ($= 14$ for PPy [28]) the relative dielectric constant of the material, $k_B$ the Boltzmann constant. The exponential decay, $\alpha^{-1}$, of the localized states was assumed to be equal to the length of three PPy rings (≈1 nm). The density of the states at the Fermi energy, $N_F$, is given by [29]

$$N_F = 40 B_C \frac{\alpha^3}{\pi k_B T_0}, \quad (4)$$

where $40B_C$ is a parameter depending on the dimensionality of the conductive network and about 19 for 3D-VRH [29]. The transition temperature was estimated to be ≈75 K for the sample with $M_n = 62,100$ and MR = 1.00, using the value of $N_F$ calculated with Eq. (4). This is almost equal to the temperature where the transition in the transport mechanism is observed in the log[$W(T)$] vs. log($T$) plots.

### 3.5. Charge transport in slightly sulfated PPy/s-PHE

No break point was observed in the log[$W(T)$] vs. log($T$) plot in the slightly sulfated samples. The single $n$ values in the range 1.7–2.3 were defined for these samples over the whole temperature range. The $n$ value smaller than two indicates the involvement of a conduction mechanism whose reduced activation energy has larger temperature dependence than that characterized by $n = 2$. Therefore, the temperature dependence of the conductivity for these samples is analyzed, assuming that the conduction consists of two components at each temperature. The dominant one is the same with that observed in the moderate sulfation region: the 2D-VRH above 80 K and the Coulomb-gap-governed one below 80 K. The other is the hopping between the nearest-neighboring localized states (NNH), that shows the $n = 1$ dependence [8]. The assumption of the NNH is justified for the samples with low MR and low PPy content. Thus, the total conductivity is approximated as

$$\sigma(T) = \sigma_0 \exp[-(T_0/T)^{1/n}] + \sigma_{NNH} \exp(-E_A/k_B T), \quad (5)$$

where the first term on the right side represents the 2D-VRH above 80 K and the Coulomb-gap-governed hopping below 80 K, and the second the NNH. The parameters in this equation, such as $\sigma_0$, $T_0$ and $E_A$, were optimized with the least-square method, and are given in Table 1.

Fig. 5 shows the simulated and the experimental results, where the thick curve is the best fit of Eq. (5) to the experimental results (open circles) and the thin straight line the NNH part in Eq. (5). The ratio of the NNH conductivity with respect to the total conductivity is about 18–40% at 270 K, depending on $M_n$ and MR, and increases with decreasing temperature. The contribution of the NNH is maximal around 130–160 K. This contribution decreases with further decrease in temperature, and below 40 K, becomes negligible. At these temperatures the thermal energy is too small for the charge carriers to be activated and hop to a nearest-neighboring state of different energy.

### 3.6. Spatial distribution of PPy chains as a function of s-PHE molecular mass

Most blends with small $M_n$ are categorized into the moderate sulfation, whereas blends with large $M_n$ are categorized into the high, moderate or low sulfation, depending upon MR. This is shown by the range of the $n$ value observed above 80 K. It is in the range 1.72–8.82 for $M_n = 151,000$, whereas it is in the range 2.87–3.02 for $M_n = 8500$ except for the ($M_n = 8,500$, MR = 1.00). A preliminary estimation of the PPy inter-chain distance reveals that all the samples would be in the moderate sulfation region and the 2D-VRH would be observed, if the PPy chains were distributed at random to form 2D channels on the s-PHE surfaces. Therefore, it can be concluded for the blends, with large $M_n$ in particular, that a part of PPys is distributed inhomogeneously. This behavior can qualitatively be

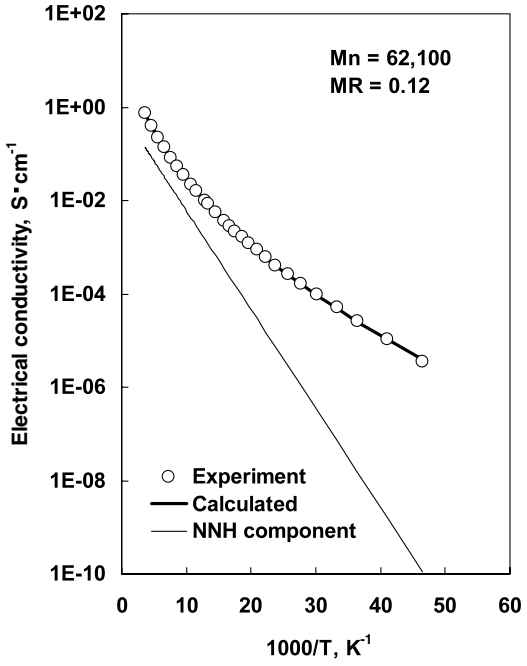


Fig. 5. The electrical conductivity of the sample with $M_n = 62,100$ and MR = 0.12 as a function of reciprocal temperature. The thick line is the best fit of Eq. (5) to the experimental results, where the *n* value in the first term is assumed to be three and two above and below 80 K, respectively. The thin straight line expresses the nearest-neighbor hopping component.

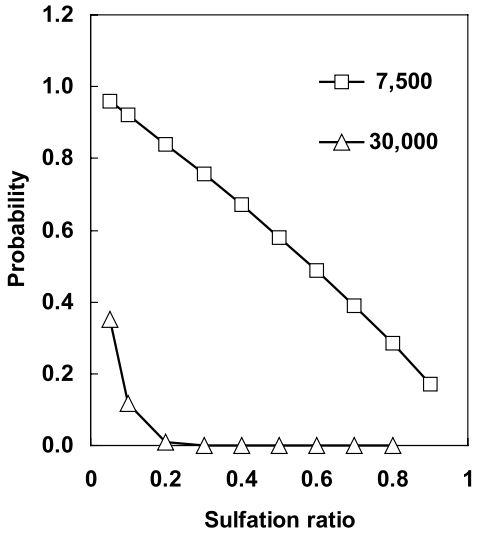


Fig. 6. The probability as a function of MR that the sulfated segments occupy surface lattice sites of the s-PHE sphere. The open squares and open triangles are the result of the estimation for $M_n = 7500$ and 30,000, respectively.

explained by taking into account the $M_n$ dependence of the spatial distribution of the sulfated hydroxy groups in the s-PHE.

The spatial distribution of the sulfated segments is first examined, by employing a 3D-lattice model, similar to the Flory–Huggins's 2D-model [30]. In the model employed, it is assumed that sulfated and unsulfated segments of a s-PHE occupy lattice sites in the 3D lattice, and are assembled to form a sphere. It is also assumed that the occupancy probability of a sulfated segment does not depend on its position in the sphere. Then the probability, $P_S$, that the sulfated segments occupy the sites on the surface of the assembled sphere is approximated by the following equation

$$P_S = \frac{N_{OUTERMOST}!}{(N_{OUTERMOST} - n_S)!n_S!} \Big/ \frac{N!}{(N - n_S)!n_S!}, \quad (6)$$

where $N$ stands for the number of the sites in the assembled PHE sphere, $n_S$ (=MR·$N$) for the number of the sulfated segment. $N_{OUTERMOST}$ is the number of the sites available on the surface of the assembled sphere, which is approximately given by

$$N_{OUTERMOST} = \frac{\frac{4}{3}\pi R^3 - \frac{4}{3}\pi(R - 2r)^3}{v}, \quad (7)$$

where $R$ is the radius of an assembled sphere, $r$ and $v$ the radius and the volume of a component sphere occupied by the sulfated- or the unsulfated-segment. The estimated probability is shown as a function of MR in Fig. 6, where the open squares and open triangles are the results for $M_n$ = 7000 and 30,000, respectively.

The probability that the sulfated segments occupy the sites on the s-PHE surface is a slowly decreasing function of MR when $M_n$ is small, whereas it decreases rapidly for large $M_n$. This means that the number of the sulfated segments in the inner region of the sphere increases rapidly with increasing MR when $M_n$ is large.

A PPy chain tends to be situated close to a sulfated segment due to the electrostatic interaction between them, if the sulfated segment is near the s-PHE surface. However, the number of the PPy chains that are not situated close to sulfated segments increases as MR increases, because more sulfated segments occupy the inner sites and it is difficult for PPy chains to penetrate into PHE spheres. The PPy distribution, then, can be inhomogeneous near the PHE-surface region because of immiscibility due to molecular mass difference between PPy and PHE. This situation is much more remarkable for large $M_n$ owing to the larger difference in the molecular mass. This may bring the region where the PPy content is high enough for the metallic phase to be formed at high MR and, at low MR, the long inter-chain distance with which only the NNH is available.

## 4. Conclusion

The doping or sulfation ratio and the molecular mass of PHE were systematically varied in the PPy/s-PHE blends to modify the geometry of the PPy conducting channels. Several types of transport mechanisms could be brought into operation reflecting the change in the parameters of the conducting channels. The blends investigated can be categorized into three groups: slight-, moderate- and

high-sulfation groups. In the moderate sulfation region, the blends are visualized as an assembly of coiled s-PHE along whose surface the 2D conducting PPy channels are formed. Their charge transport above 80 K, therefore, is the 2D-VRH. As MR is increased, the dimensionality of the VRH changes from 2D to 3D. In addition, the charge carriers in the metallic states also participate in the transport in parallel with the 3D-VRH. On the contrary, as MR is decreased, the hopping to the nearest neighbors is in operation as well as the VRH. The dominant conduction below 80 K for all the samples is the hopping one governed by a Coulomb gap due to the electrostatic interaction between the carriers. The emergence of various transports was qualitatively explained in terms of the inhomogeneous PPy distribution as a function of $M_n$.

## References


[1] Mott NF, Davis EA. Electronic processes in non-crystalline materials. 2nd ed. Oxford: Clarendon Press, 1979.
[2] Mott NF. Conduction in non-crystalline materials. Oxford: Oxford University Press, 1987.
[3] Hamilton EM. Philos Mag 1972;26:1043–5.
[4] Efros AL, Shklovskii BI. J Phys C: Solid State Phys 1975;8:L49–51.
[5] Sheng P, Abeles B, Arie Y. Phys Rev Lett 1973;31(1):44–47.
[6] Sheng P, Klafter J. Phys Rev B 1983;27(4):2583–6.
[7] Bloch AN, Weisman RB, Varma CM. Phys Rev Lett 1972;28(12):753–6.
[8] Miller A, Abrahams E. Phys Rev 1960;120(3):745–55.
[9] Wernet W, Yamato H, Kai K, Koshiba T, Ohwa M. Solid State Ionics 1992;53-56:1125–31.
[10] Yamato H, Wernet W, Ohwa M, Rotzinger B. Synth Met 1993;55–57:3550–5.
[11] Zuppiroli L, Bussac MN, Paschen S, Chavet O, Forro L. Phys Rev B 1994;50(8):5196–203.
[12] Glatzhofer DT, Ulañski J, Wegner G. Polymer 1987;28:449–53.
[13] Ulañski J, Glatzhofer DT, Przybylski M, Kremer F, Gleitz A, Wegner G. Polymer 1987;28:859–62.
[14] Watanabe A, Tanaka M, Tanaka J. Bull Chem Soc Jpn 1981;54(8):2278–81.
[15] Roy R, Sen SK, Digar M, Bhattacharyya SN. J Phys Condens Matter 1991;3:7849–56.
[16] Singh R, Tandon RP, Chandra SJ. Appl Phys 1991;70(1):243–5.
[17] Meikap AK, Das A, Chatterjee S, Digar M, Bhattacharyya SN. Phys Rev B 1993;47(3):1340–5.
[18] Singh R, Narula AK, Tandon RP, Mansingh A, Chandra S. J Appl Phys 1996;79(3):1476–80.
[19] Sato K, Yamaura M, Hagiwara T, Murata K, Tokumoto M. Synth Met 1991;40:35–48.
[20] Travers JR, Audebert P, Bidan G. Mol Cryst Liq Cryst 1985;118:149–53.
[21] Nalwa HS. J Mater Sci 1992;27:210–4.
[22] Maddison DS, Tansley TL. J Appl Phys 1992;72(10):4677–92.
[23] Zabrodskiĭ AG, Zinov'eva KN. Sov Phys JETP 1984;59(2):425–33.
[24] Cowie JMG. Polymers:chemistry and physics of modern materials. 2nd ed. Glasgow: Blackie and Son, 1991.
[25] Roth S. Mater Sci Forum 1989;42:1–16.
[26] Cervini R, Fleming RJ, Murray KS. J Mater Chem 1992;2(11):1115–21.
[27] Yumoto Y, Yoshimura S. Synth Met 1986;13:185–91.
[28] Salmon M, Kanazawa KK, Diaz AF, Krounbi M. J Polym Sci: Polym Lett Ed 1982;20:187–93.
[29] Shante VKS. Phys Rev B 1977;16(6):2597–612.
[30] Krause S. In: Paul DR, Newman S, editors. Polymer blend, vol. 1. New York: Academic Press, 1978.